Available online at www.sciencedirect.com
SCIENCE DIRECT
Applied Catalysis A: General 309 (2006) 76–84
APPLIED CATALYSIS A: GENERAL
www.elsevier.com/locate/apcata

$K_4Ce_2M_{10}O_{30}$ (M = Ta, Nb) as visible light-driven photocatalysts for hydrogen evolution from water decomposition

Mengkui Tian [a,b,c], Wenfeng Shangguan [a,*], Jian Yuan [a], Li Jiang [a], Mingxia Chen [a], Jianwei Shi [a], Ziyuan Ouyang [b], Shijie Wang [b]

[a] *Research Center for Combustion and Environment Technology, Shanghai Jiao Tong University, Shanghai 200030, PR China*
[b] *Geochemistry Institute of Chinese Academy of Sciences, Guiyang, Guizhou 550002, PR China*
[c] *Graduate School of Chinese Academy of Sciences, Beijing 100047, PR China*

Received 4 January 2006; received in revised form 1 April 2006; accepted 24 April 2006
Available online 2 June 2006

Abstract

A series of single-phase metal oxide photocatalysts $K_4Ce_2M_{10}O_{30}$ (M = Ta, Nb), capable of evolving H_2 and O_2 from aqueous solutions containing a sacrificial electron donor (Na_2SO_3) and acceptor ($AgNO_3$), respectively, under visible light irradiation ($\lambda > 420$ nm) without any co-catalyst were presented. The activities were greatly enhanced by the incorporation of Pt, RuO_2 and NiO (NiO_x) as co-catalysts on the prepared oxides. The photocatalysts have an appropriate band gap energy *ca*. 1.8–2.3 eV (corresponding to absorption edge of 540–690 nm) and excellent chemical potential level for utilization of solar energy, representing candidates of photocatalysts for hydrogen evolution from water decomposition. Density function theory (DFT) calculation indicated that while their valence bands are composed of hybridization with O 2p + Ta 5d (or Nb 4d) and occupied Ce 4f orbitals, the conduction bands of these photocatalysts $K_4Ce_2M_{10}O_{30}$ (M = Ta, Nb) are mainly attributable to the Ta 5d (or Nb 4d) orbitals. Although the unoccupied Ce 4f orbitals have overlap in the bottom of conduction band, they are less effective in transferring electrons and photocatalytic activities for their high localized nature. The contribution of these orbitals to the energy bands affects the electronic structure of the both photocatalysts and gives rise to their differences in light absorption and photocatalytic activities.

Keywords: Photocatalyst; Visible light-driven; $K_4Ce_2M_{10}O_{30}$ (M = Ta, Nb); Water decomposition; DFT calculation

1. Introduction

Since the evolution of hydrogen and oxygen on TiO_2 and Pt counter electrodes under the irradiation of ultraviolet (UV) light was reported by Fujishima and Honda in 1972 [1], photocatalysis has been received much attention and widely studied with the aim of efficiently converting solar energy into clean hydrogen energy. Up to now, these compounds locating in d block possessing d^0 electronic configuration [2–5], such as $SrTiO_3$, $K_4Nb_6O_{17}$, $ATaO_3$ (A = Li, Na, K), $A_2Ta_2O_6$ (A = Ca, Sr, Ba) and $Cs_2Nb_4O_{11}$, and these locating in p block possessing d^{10} electronic configuration [6,7], such as MIn_2O_4 (M = Ca, Sr), Sr_2SnO_4, $NaSbO_3$ and Zn_2GeO_4 were intensively studied. Most of them showed high stability and activities. However, these photocatalysts are only active under UV light, which accounts for only about 5% of the solar spectrum at the earth's surface. Therefore, the development of visible light responsive photocatalysts for water decomposition is currently attracting much attention as a potentially efficient utilization of solar energy. Although some photocatalysts, such as WO_3 and $BiVO_4$, have shown O_2 evolution from $AgNO_3$ solution under visible light irradiation, such materials have not exhibited reduction of H^+ into H_2 because their conduction bands do not have sufficient potentials for H_2 evolution [8]. Many metal sulfides have the narrower band gaps that correspond to the visible light absorption, but it is commonly believed that metal sulfides are unstable in aqueous solutions under irradiation due to electrochemical dissolution. Although incorporation of CdS into some layered metal oxides was efficient for stabilizing the metal sulfides and producing hydrogen from water [9], the preparation procedure is complicated and the photocatalytic efficiency is still low. Moreover, many band engineering methods were also

* Corresponding author. Tel.: +86 21 64076226; fax: +86 21 64075359.
E-mail address: shangguan@sjtu.edu.cn (W. Shangguan).

0926-860X/$ – see front matter
doi:10.1016/j.apcata.2006.04.035

extensively studied to extend their absorption edges to visible light, such as solid solution, transition metal cation and anion doping [10]. The solid solution ($Ga_{1-x}Zn_x$) ($N_{1-x}O_x$) derived from GaN and ZnO [11], as well as co-doped TiO_2 and $SrTiO_3$ with Sb^{5+} and Cr^{3+}, Ni^{2+}, Cu^{2+} showed visible light responsive properties [12]. Since Asahi et al. [13] reported that nitrogen doping of TiO_2 ($TiO_{2-x}N_x$) extended its light absorption to visible light range ($\lambda < 500$ nm), some metal nitrides and oxynitrides, such as TaON ($\lambda < 500$ nm) [14], Ta_3N_5 ($\lambda < 600$ nm) [15] and $Y_2Ta_2O_5N_2$ ($\lambda < 560$ nm) [16] as well as other anion doping (S [17], C [18], etc.) have been developed as visible light sensitive photocatalysts. However, there is a concern for the stability of substituted anions under reaction conditions for the compounds, so the most promising candidates for photocatalysts under visible light are single-phase metal oxides [19]. In order to develop new photocatalysts, some of compounds including rear earth elements have been received great attention. $RbLnTa_2O_7$ (Ln = La, Pr, Nd, Sm) [20] have been studied for water splitting and showed excellent stability and high activity under UV light. Although Bi_2RNbO_7 (R = La, Pr, Nd, Sm, Gd, Ce) [21] exhibited absorption in the visible region, the absorption range remained limited and did not show photocatalytic activities under visible light. Kudo et al. [22] have reported in letter the water splitting activities of $K_2LnTa_5O_{15}$ (also denoted as $K_4Ln_2Ta_{10}O_{30}$) [23] under UV light. It should be noted that as only Ln = Ce among these series of the photocatalysts exhibits absorption in the visible region, implying the potential for decomposing water for hydrogen evolution under visible light. Our current paper focused on the photocatalytic activities of $K_4Ce_2M_{10}O_{30}$ (M = Ta, Nb) for hydrogen evolution from water using visible light ($\lambda > 420$ nm) and the loading of Pt, RuO_2 and NiO (NiO_x) for the promotion of photocatalytic activity. The feature of their electronic structure and its influence on the activities was also analyzed based on density function theory (DFT) first principle calculation.

2. Experimental

2.1. Preparation and characterization of materials

$K_4Ce_2M_{10}O_{30}$ (M = Ta, Nb) were synthesized from high purity of $K_2CO_3{\cdot}3H_2O$, $Ce(NO_3)_3{\cdot}6H_2O$, Ta_2O_5 (or Nb_2O_5) through conventional high temperature solid-state reactions, first at 800 °C for 5 h then 1100 °C for 12 h, with a regrounding process in between. Excess $K_2CO_3{\cdot}3H_2O$ (*ca.* 20%) was used to compensate for the loss caused by volatilization during calcination. After the reaction, the product was washed with distilled water and dried. Pt was photodeposited on the $K_4Ce_2M_{10}O_{30}$ catalysts in situ from precursor of $H_2PtCl_6{\cdot}6H_2O$, and RuO_2 was loaded by impregnation of $RuCl_3{\cdot}3H_2O$ and then calcinated at 500 °C in atmosphere, as reported [9]. The 1.0 wt% NiO-loaded photocatalysts were obtained through calcination at 350 °C for 1 h in air after drying the mixture of powder samples with aqueous $Ni(NO_3)_2$ solution at 80 °C. As-prepared photocatalysts loaded with NiO were further reduced in H_2 atmosphere at 500 °C for 2 h, then, treated in air atmosphere at 200 °C for 1 h. The samples followed with this reduction–oxidation procedure were denoted as NiO_x loading [21].

The resulting samples were identified by X-ray diffraction on Bruker-AXS D8 Advance with Cu Kα radiation (λ = 1.54178 Å). XRD data were collected with a step scan procedure in the range of $2\theta = 5$–80°. The step interval was 0.02° and scan speed was 4° min^{-1}. The TEM was recorded on JEM1200EX with accelerating voltage of 80 kV. The BET surface areas of the $K_4Ce_2M_{10}O_{30}$ (M = Ta, Nb) powders were determined from N_2 adsorption–desorption isotherm on Quantachrome NOVA 1000-TS. UV–vis diffuse reflectance spectra were measured using TU-1901 spectrophotometer. The reflectivity spectrum was transformed to absorbance intensity through Kubelka–Munk method.

2.2. Measurement of photocatalytic activity

The photocatalytic reaction was carried out in a photoreactor [9], which was provided with an entry window of optical flat quartz glass of *ca.* 64.0 cm^2. 0.1 g of photocatalyst powder was dispersed and suspended in 20 mL of aqueous solution in the reactor under the vertical irradiation with 300 W Xe lamp. A series of cut-off filter glasses were used to make specific wavelength area effective to photocalytic activity. In order to detect the photocatalytic activity under visible light, a glass cut-off filter ($\lambda > 420$ nm) was used to remove UV light. H_2 and O_2 evolution was measured by gas chromatography (QC-9101) with thermal conductivity detector (TCD) and Ar as carrier gas.

3. Results and discussion

3.1. Characterization of materials

The resulting powders of $K_4Ce_2M_{10}O_{30}$ (M = Ta, Nb) had an X-ray diffraction pattern consistent with the tetragonal tungsten bronze structured [23], being with the parallelepiped morphological structure. As the almost same ion radius of Ta^{5+} (0.68 Å) and Nb^{5+} (0.69 Å), both (M = Ta, Nb) usually presented the isostructure compounds. Their XRD spectrums were shown in

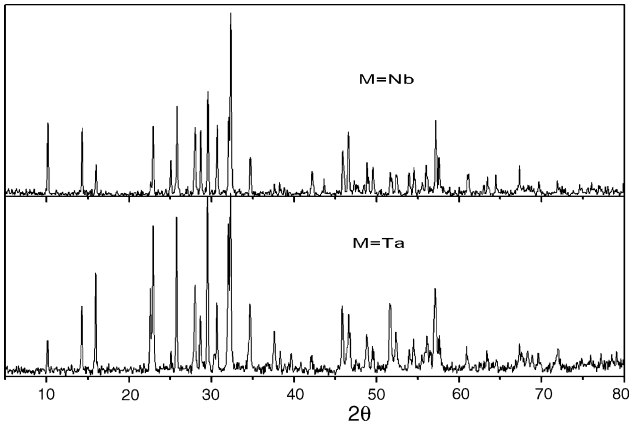

Fig. 1. XRD patterns for $K_4Ce_2M_{10}O_{30}$ (M = Ta, Nb).

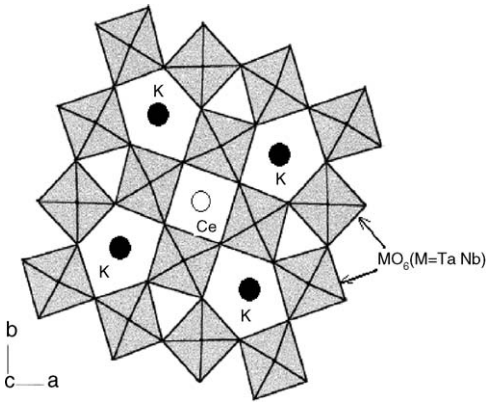

Fig. 2. Schematic crystal structure of $K_4Ce_2M_{10}O_{30}$ (M = Ta, Nb).

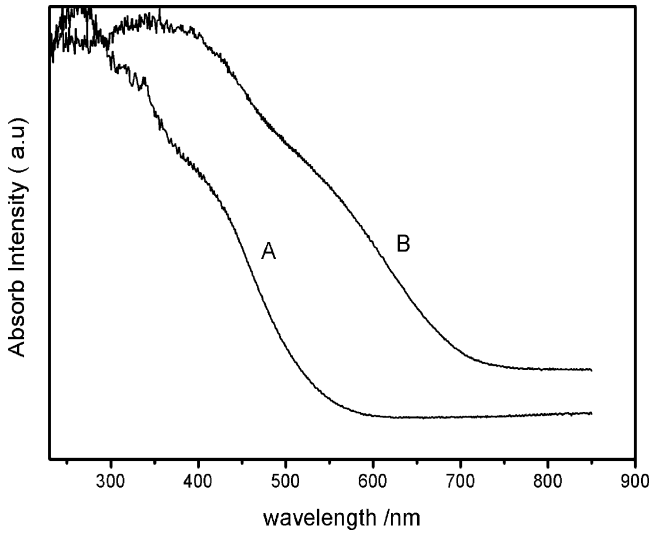

Fig. 3. UV–vis diffuse reflection spectra of $K_4Ce_2M_{10}O_{30}$ for (A) M = Ta and (B) M = Nb.

Fig. 1, indicating that their peak position and intensity are almost the same. The schematic for their crystal structure was shown in Fig. 2, in which corner-shared TaO_6 (NbO_6) octahedra provides three kinds of tunnels with pentagonal, square and trigonal sections extending in the direction of the 0 0 1, and the K atoms are distributed in the pentagonal tunnels while the Ce atoms are inserted into the square tunnels.

The UV–vis diffuse reflectance spectra of $K_4Ce_2M_{10}O_{30}$ (M = Ta, Nb) were shown in Fig. 3. The absorption edge of $K_4Ce_2Ta_{10}O_{30}$ is at about 540 nm, corresponding to a band gap energy of 2.3 eV; and the absorption edge of $K_4Ce_2Nb_{10}O_{30}$ is at about 690 nm, corresponding to a band gap energy of 1.8 eV. Their absorption properties are consistent with their appearance colors (golden yellow in color for $K_4Ce_2Ta_{10}O_{30}$, while $K_4Ce_2Nb_{10}O_{30}$ appeared deep brown in color). The as-prepared $K_4Ce_2M_{10}O_{30}$ (M = Ta, Nb) catalysts present a band gap energy near 2.0 eV, which is regarded as a very appropriate level for photocatalytic water splitting [10].

3.2. Photocatalytic H_2 and O_2 evolution on $K_4Ce_2M_{10}O_{30}$ (M = Ta, Nb)

The time course of H_2 evolution in aqueous Na_2SO_3 solution under visible light ($\lambda > 420$ nm) were showed in Fig. 4, which indicates H_2 evolved steadily during the irradiation time more than 72 h. No noticeable differences were observed in the X-ray diffraction patterns for the both catalysts before and after reaction. The turnover number [24] of the evolved H_2 to the amount of photocatalyst reached 9.6 and 1.4 for M = Ta and M = Nb, respectively, in 72 h reaction under visible light irradiation. Combined with the results of control experiment for the investigation of H_2 evolution on Na_2SO_3 solution without the presence of catalysts, which almost did not show response on the peak position of H_2 appearance, it can be confirmed that

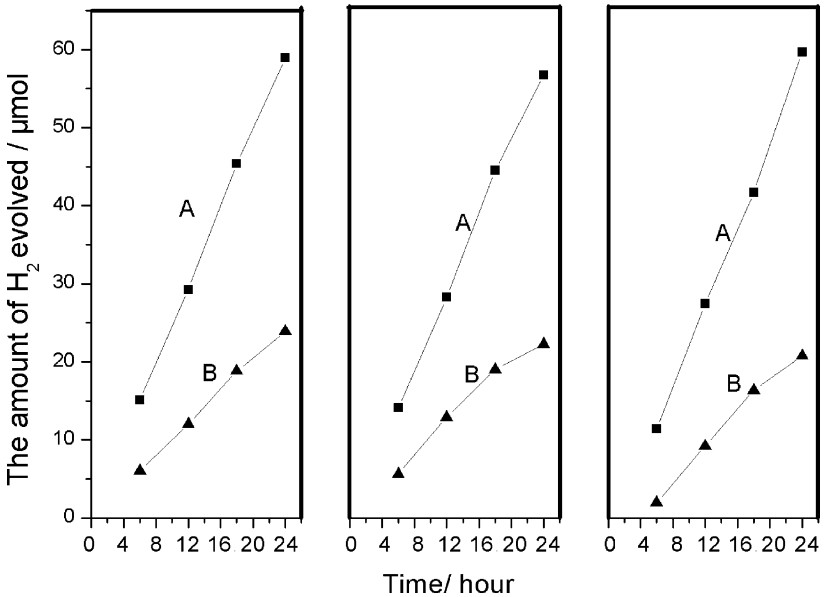

Fig. 4. H_2 evolution on $K_4Ce_2M_{10}O_{30}$ for M = Ta (line A) and M = Nb (line B) in 0.2 M Na_2SO_3 aqueous solution (20 mL): catalyst, 0.1 g; light source, 300 W Xe lamp with $\lambda > 420$ nm filter.

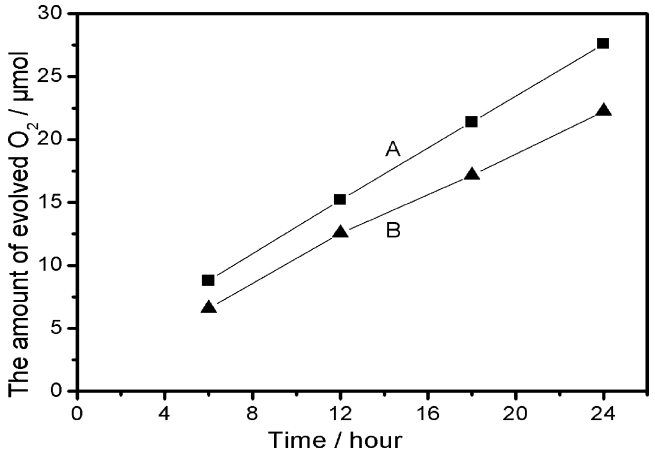

Fig. 5. O_2 evolution on $K_4Ce_2M_{10}O_{30}$ for M = Ta (line A) and M = Nb (line B) in 0.02 M $AgNO_3$ solution (50 mL): catalyst, 0.2 g; light source, 300 W Xe lamp with $\lambda > 420$ nm filter.

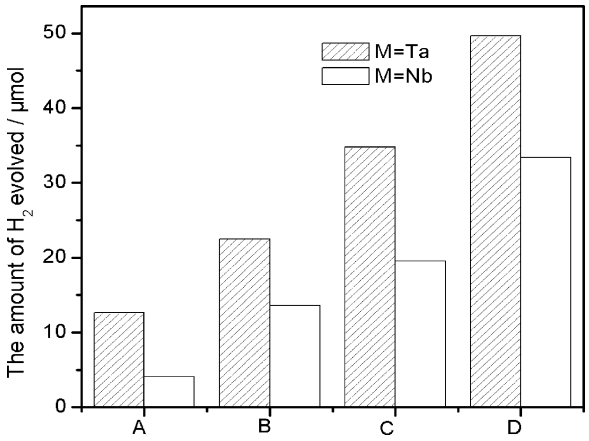

Fig. 7. The rate of H_2 evolution on $K_4Ce_2M_{10}O_{30}$ (M = Ta, Nb) catalysts without loading (A), with loading of 0.3 wt% Pt (B), 1.0 wt% RuO_2 (C) and 0.3 wt% Pt–1.0 wt% RuO_2 (D) in 0.2 M Na_2SO_3 aqueous solution (20 mL): catalyst, 0.1 g; light source, 300 W Xe lamp with filter ($\lambda > 420$ nm) for 4 h.

the reaction of H_2 evolution on $K_4Ce_2M_{10}O_{30}$ (M = Ta, Nb) occurs catalytically.

The requirements for the overall photocatalysis process lie in the following electrochemical conditions. The chemical potential level of photoinduced electron is more negative than that of the potential for reducing H_2O to H_2 and the potential of photoinduced holes is more positive than that for oxidizing H_2O to O_2, which also means that the position of a semiconductor photocatalyst's bottom of conduction band need to be higher than the level of H^+/H_2 (NHE = 0) while the position of top of valance band to be lower than the level of O_2/H_2O (NHE = +1.23 V), for the higher position of conduction band and the lower of valance band are, the more powerful redoxing ability they have. In order to make sure whether the position of valence band of these photocatalysts is lower than that of O_2/H_2O and whether has enough positive chemical potential to oxidizing H_2O to O_2 or not, 0.02 M $AgNO_3$ was used as electron acceptor for the photocatalytic oxidation of water. The experiment of O_2 evolution was carried out under visible light ($\lambda > 420$ nm). No reaction took place for long time in the absence of either light or photocatalyst. Upon irradiation for the photocatalytic system, O_2 was examined, and about 28.0 and 22.5 μmol were evolved in 24 h for $K_4Ce_2Ta_{10}O_{30}$ and $K_4Ce_2Nb_{10}O_{30}$, respectively (Fig. 5). The finding indicates that the photocatalysts have an appropriate band levels for the reduction and oxidation of water into hydrogen and oxygen [16].

3.3. Loading with Pt, RuO_2 and NiO (NiO_x) on $K_4Ce_2M_{10}O_{30}$ (M = Ta, Nb)

Usually, some noble metals and its metal oxides are used to prompt the photocatalytic activities acting as co-catalysts. In order to evaluate the effect of co-catalysts on the photocatalytic activity, the evolution of hydrogen on $K_4Ce_2M_{10}O_{30}$ (M = Ta, Nb) with loading of Pt or RuO_2 were carried out under visible light ($\lambda > 420$ nm). The variation in photocatalytic activities with the amount of Pt or RuO_2 loading is shown in Fig. 6. Both of the loading of Pt and RuO_2 prompted obviously the H_2 evolution activities on $K_4Ce_2M_{10}O_{30}$ (M = Ta, Nb). The promotion is attributable to facilitate electron migrating from

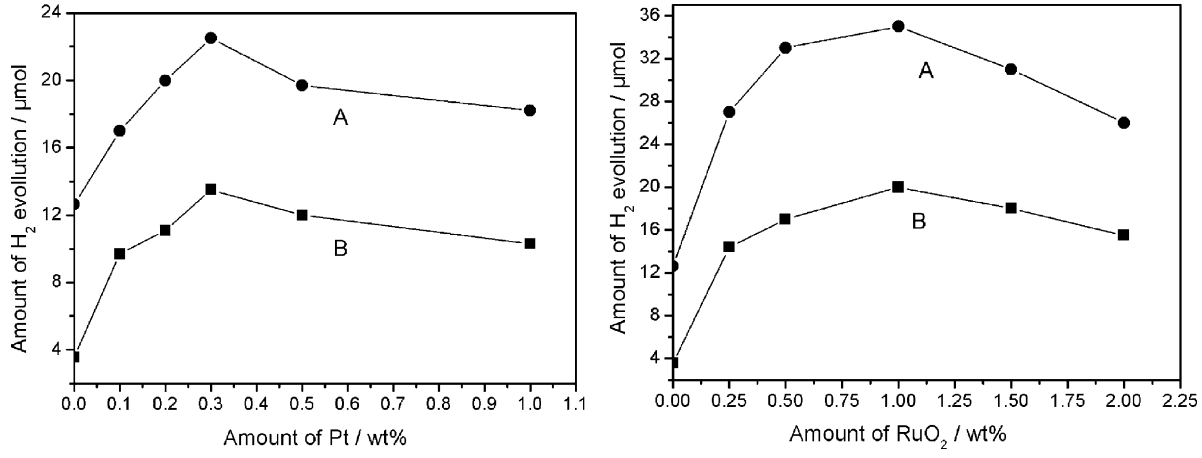

Fig. 6. Variation in the photocatalytic activity for H_2 evolution on $K_4Ce_2M_{10}O_{30}$ for M = Ta (A) and M = Nb (B) with the loading amount of Pt (a) and RuO_2 (b) in 0.2 M Na_2SO_3 solution (20 mL): catalyst, 0.1 g; light source, 300 W Xe lamp with filter ($\lambda > 420$ nm) for 4 h.

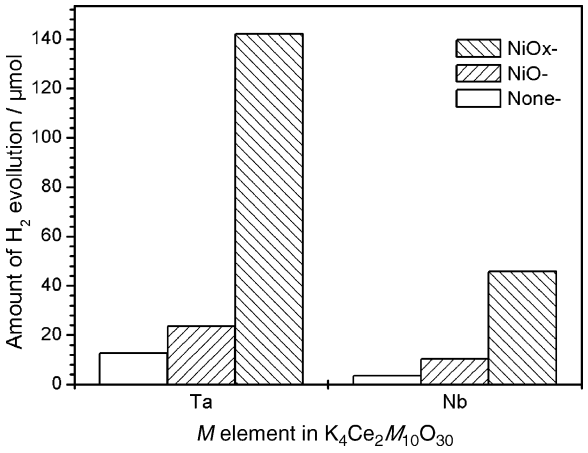

Fig. 8. The activities for H_2 evolution on $K_4Ce_2M_{10}O_{30}$ (M = Ta, Nb) without loading and with loading of 1.0% NiO and NiO_x in 0.2 M Na_2SO_3 aqueous solution (20 mL): catalyst, 0.1 g; light source, 300 W Xe lamp with filter ($\lambda > 420$ nm) for 4 h.

the conduction band of $K_4Ce_2M_{10}O_{30}$ (M = Ta, Nb) to the Pt and RuO_2 nanoparticles, which function as H_2 production sites on the surface of catalysts [11]. The parallelepiped (tunnel) surface structure of $K_4Ce_2M_{10}O_{30}$ (M = Ta, Nb) is beneficial to the formation of ''nest'' [25], where nanoparticles of Pt and RuO_2 are strongly associated, improving the photocatalytic activity greatly. Additionally, the activities increased with the amount of loading, reaching a maximum at 0.3 wt% for Pt and 1 wt% for RuO_2, and then decreased with further loading. This might be due to the excess of Pt or RuO_2 loading reduced the density of active sites and inhibited the optical absorption properties. Thus, there appeared a maximum in the curve of the activities versus the amount of the loading [26]. As shown in Fig. 7, the activity was further increased by co-depositing both Pt and RuO_2 on the catalysts. This rate is four to eight times greater than those without any loading. The synergic effect of Pt and RuO_2 was presented in the promotion of the activities for photocatalytic hydrogen evolution.

It has been well believed that loading of NiO (or NiO_x) as co-catalyst prompted photocatalytic activities markedly [27–30].

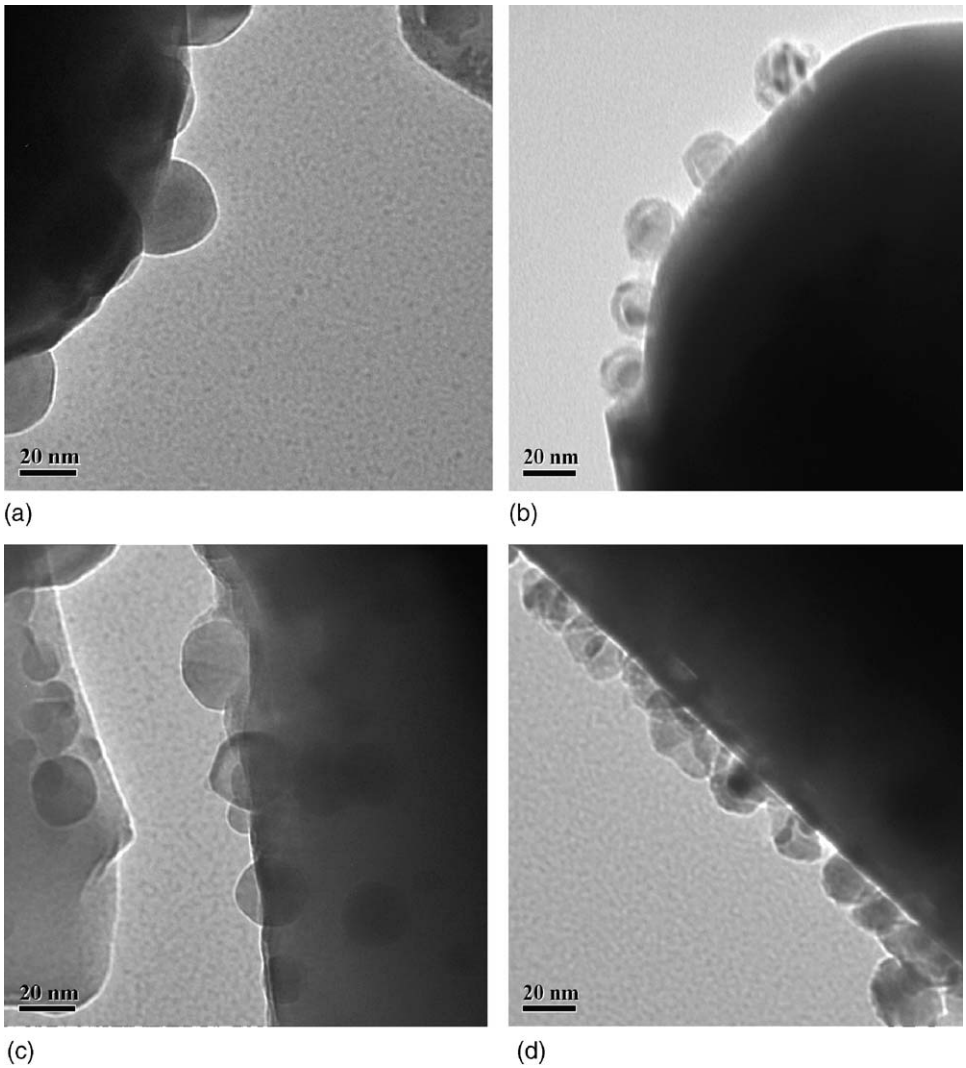

Fig. 9. TEM images for NiO (a) and NiO_x (b) anchoring on $K_4Ce_2Ta_{10}O_{30}$, and NiO (c) and NiO_x (d) anchoring on $K_4Ce_2Nb_{10}O_{30}$, respectively.

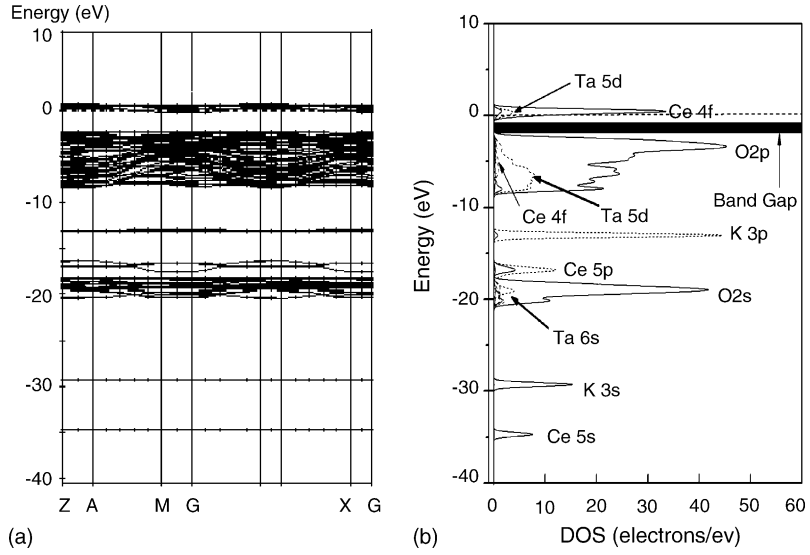

Fig. 10. Energy-band diagram (a) and density of states (b) for $K_4Ce_2Ta_{10}O_{30}$ calculated by a DFT method.

We prepared both of NiO and NiO_x loading on $K_4Ce_2M_{10}O_{30}$ (M = Ta, Nb) to investigate the effect of such co-catalysts. Their photocatalytic H_2 evolution activities under visible light ($\lambda > 420$ nm) were shown in Fig. 8. It is found that NiO_x loading is superior to NiO loading with respective to promoting the activity, while the both loading enhanced the hydrogen evolution under visible irradiation. The amount of H_2 evolution for 4 h on NiO_x-loaded $K_4Ce_2Ta_{10}O_{30}$ reached 135 μmol, which is about four times of that co-loaded with Pt and RuO_2 and five times of that loaded with NiO. Fig. 9 shows the TEM images of the catalysts loaded with NiO and NiO_x. The uniform distribution of loaded particles on the surface of catalysts is ascribed to the "nest" surface structure of $K_4Ce_2M_{10}O_{30}$, where NiO and NiO_x nanoparticles are uniformly fixed. It is seen that NiO_x derived from partial reduction and oxidation procedure formed the double-layer particles including metallic Ni and NiO, while NiO formed the uniform particles anchoring on the surface of $K_4Ce_2M_{10}O_{30}$. The loaded NiO and NiO_x particles facilitate the transfer of photoinduced electron to these sites, restraining the recombination of photoinduced charges. The higher activity of NiO_x-loading compared with NiO-loading might be ascribed to the following reasons. Since the surface NiO works as a H_2 evolution site, electrons photogenerated in photocatalysts have to cross the interface between photocatalysts and loaded co-catalyst to reach the surface for reducing water. In this case, the barrier for the electron crossing the interface between heat-treated Ni metal and oxide photocatalysts seems to be lower than that at the interface between NiO and oxide photocatalysts. Thus, the double-layered structure of nickel formed by the treatment of

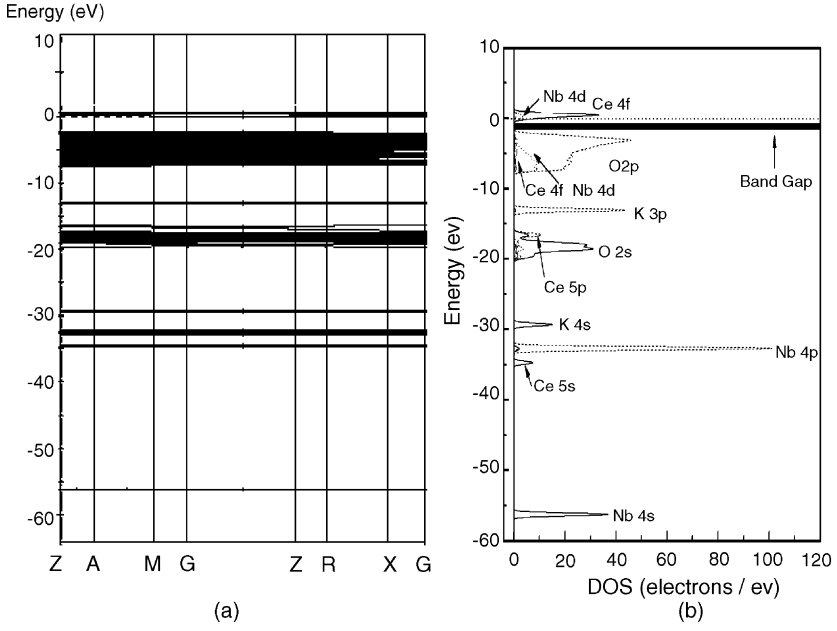

Fig. 11. Energy-band diagram (a) and density of states (b) for $K_4Ce_2Nb_{10}O_{30}$ calculated by a DFT method.

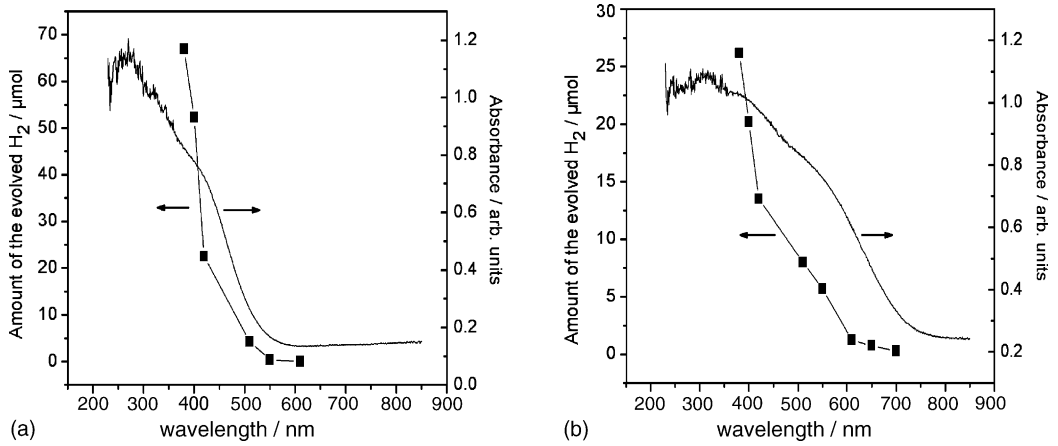

Fig. 12. Action spectra of H_2 evolution from an aqueous Na_2SO_3 solution over the Pt (0.3 wt%)-loaded $K_4Ce_2M_{10}O_{30}$ for M = Ta (a) and M = Nb (b) in 0.2 M Na_2SO_3 aqueous solution (20 mL): catalyst, 0.1 g; light source, 300 W Xe lamp with series of cut-off filters for 4 h.

reduction–oxidation is easier to assist the electron transferring from photocatalysts to co-catalysts [31].

Furthermore, in order to investigate the role of co-catalysts for the H_2 evolution, Pt (0.3 wt%), RuO_2 (1.0 wt%), NiO (1.0 wt%) and NiO_x (1.0 wt%) were loaded, respectively, by the same procedures on TiO_2 (P25), which is only active under UV light. Photocatalytic reactions were carried out in Na_2SO_3 aqueous solution under the visible light irradiation ($\lambda > 420$ nm). Hardly any evolved H_2 was examined for long time. Therefore, it can be confirmed that the H_2 evolution on $K_4Ce_2M_{10}O_{30}$ (M = Ta, Nb) loaded with Pt, RuO_2, NiO (NiO_x) in Na_2SO_3 solution under visible light irradiation is ascribed to the photocatalytic reaction.

3.4. Electronic structure of $K_4Ce_2M_{10}O_{30}$ (M = Ta, Nb)

As for tantalates and niobates, a typical semiconductor photocatalysts locating in d block possessing d^0 electronic configuration, usually their conduction band and valence bands are mainly consisting of Ta 5d (or Nb 4d) and O 2p orbitals, respectively, such as $Sr_2M_2O_7$ (M = Ta, Nb) [31]. Because of the great band gap between the chemical potential of Ta 5d (−0.9 V) or Nb 4d (−0.7 V) and O 2p (+3.0 V), their absorption range remained limited in UV light. The visible light absorption properties of other tantalates and niobates, such as $BiTaO_4$ (2.7 eV) and $BiNbO_4$ (2.6 eV), $InTaO_4$ (2.6 eV) and $InNbO_4$ (2.5 eV) result from the high chemical potential of Bi 6s and In 5s contributable to the formation of their valence bands [32,33].

Based on the analysis above, it is speculated that the property for the VIS-absorption might originate partially from the contribution of rare earth element Ce to the band gap in $K_4Ce_2M_{10}O_{30}$ (M = Ta, Nb). The first principle calculations were carried out based on density function theory with plane-wave pseudopotential method and generalized gradient approximation [34]. The core orbitals were replaced by the ultrasoft core potentials, and the O $2s^22p^4$, K $3s^23p^64s^1$, Ce $4f^15s^25p^65d^16s^2$, Ta $5d^36s^2$ and Nb $4s^24p^64d^15s^1$ electrons were treated explicitly. The kinetic energy cut-off was set at 330 eV. The energy-band structure and density of states (DOS) of $K_4Ce_2M_{10}O_3$ (M = Ta, Nb) are shown in Figs. 10 and 11. The obvious results obtained firstly are that the band gap of $K_4Ce_2M_{10}O_3$ is 1.6 eV for M = Ta and 1.1 eV for M = Nb. The band gap calculated by DFT was smaller than that obtained experimentally, which is frequently pointed out as a common feature of DFT calculations [35]. From the band structure and the partial density of states, it can be seen that the valence band of $K_4Ce_2M_{10}O_3$ (M = Ta, Nb) are made up of the O 2p, Ta 5d (or Nb 4d) and Ce 4f orbitals, and the conduction band are consisted of the Ta 5d (Nb 4d) and Ce 4f, still little degree of O 2p. Here, it should be noticed that Ce 4f was separated and laid in the valence band with lower energy level and the conduction band with higher energy level, respectively.

The effect of lanthanides elements on the band gap of semiconductors is complicated. In $RbLnTa_2O_7$ (Ln = Pr, Nd, Sm), the occupied 4f appeared to be not completely localized, but contributed partly to the hybridization with O 2p and Ta 5d [20]. It has been reported [36,37] that in the case of these later lanthanides elements, such as Gd, Tb, Dy, Ho and Er in visible light responding photocatalysts $Ln_2Ti_2S_2O_5$, the Ln 4f hybridized with O 2p and S 3p forming the valence band and S 3p + Ln 4f and Ti 3d forming the conduction band, respectively, ascribed to their lower energy levels with the increase number of 4f electrons. However, in the case of these earlier lanthanides elements, such as Pr, Nd, and Sm, Ln 4f orbitals were regarded localizing in the valence band and conduction band separately. The role of Ln 4f is dependent on their energy level and distribution of density of states, which varies with different chemical compositions and crystal structures [38]. From the band dispersion and the density of states in $K_4Ce_2M_{10}O_3$ (M = Ta, Nb), it is found that while the peak of occupied Ce 4f in the valence band is distributed broadly, the peak of unoccupied Ce 4f in the conduction band is strong and narrow, being the localized character. Thus, it may be proposed that the lower energy level of occupied Ce 4f have contribution to the valence band with Ta 5d (Nb 4d) and O 2p, while the higher energy level of unoccupied Ce 4f localized separately due to its high localized nature, which can be deduced from its high and concentrative DOS compared with other element and occupied Ce 4f. Based on above considerations and for the best of our understanding, although the

unoccupied Ce 4f orbitals appear at the bottom of conduction band, their highly localized nature in the conduction band make them less effective in photoconductivity or photocatalysis. In other words, even if the unoccupied Ce 4f orbitals accept photoexcited electrons by visible light irradiation, it is less effective in transferring those electrons to the catalyst surface due to their highly localized nature, as reported for $Ln_2Ti_2S_2O_5$ [36,37].

It is noticed that the absorption edges of the prepared photocatalysts $K_4Ce_2M_{10}O_{30}$ (M = Ta, Nb) are not steep, compared with some typical photocatalysts, such as TiO_2. In order to ascertain the relation between light absorption and photocatalytic activity, the action spectra for photocatalytic hydrogen evolution on $K_4Ce_2M_{10}O_{30}$ (M = Ta, Nb) under visible light were drawn (Fig. 12). With the increase of cut-off wavelength, the rates of H_2 evolution decreased due to the deduction of the absorption of photons. The onset of action spectra agreed with that of the diffuse reflection spectra. Therefore, it can be concluded that these photoreactions are proceeding via band gap transition, judging by the good consistence of the action spectra with the diffuse reflectivity spectra. Although the reason is still not clear, the curve aspect of absorption edges might result from the characteristic of their electronic structure. Similar absorption peculiarity was also found in other visible light-driven photocatalysts, such as $InVO_4$, $InNbO_4$ and $InTaO_4$ [39].

It is also noted that the activities for H_2 evolution on $K_4Ce_2Ta_{10}O_{30}$ are more excellent than that on $K_4Ce_2Nb_{10}O_{30}$ (as seen in Figs. 4 and 6), although the band gap of $K_4Ce_2Nb_{10}O_{30}$ (1.8 eV) is narrower than that of $K_4Ce_2Ta_{10}O_{30}$ (2.3 eV) and the BET surface area of M = Ta (1.67 m^2/g) is smaller than that of M = Nb (2.65 m^2/g). It is suggested that the difference in the photocatalytic properties between the both compounds is mainly due to the difference in their band structure rather than their difference in light absorption and surface properties [31]. This could be ascribed to the following reasons. While the both photocatalysts have the almost same level in the top of valence band, the bottom of conduction band for $K_4Ce_2Nb_{10}O_{30}$ locates too close to the NHE potential (H^+/H_2 level) due to Nb 4d level is lower than that of Ta 5d, resulting in the driving force for water reduction is smaller correspondingly.

4. Conclusions

In summary, $K_4Ce_2M_{10}O_{30}$ (M = Ta, Nb) are presented as novel metal oxide photocatalysts with an appropriate band gap energy *ca*. 1.8–2.3 eV for utilization of solar energy, exhibiting high activity for the reduction and oxidation of water into H_2 and O_2 in the presence of sacrificial electron donor or acceptor under the irradiation of visible light. This activity is enhanced by the incorporation of Pt, RuO_2 and NiO (or NiO_x) as co-catalysts. Especially, the NiO_x loading with partial reduction and oxidation pretreatment procedure forming the Ni metal and NiO oxide double layer structure prompted the photocatalytic H_2 evolution most significantly. The conduction bands of these photocatalysts $K_4Ce_2M_{10}O_{30}$ (M = Ta, Nb) are mainly attributable to the Ta 5d (or Nb 4d) orbitals, while their valence bands are composed of hybridization with O 2p + Ta 5d (or Nb 4d) and occupied Ce 4f orbitals, which makes an essential contribution to the small band gap energy of these photocatalysts. Although the unoccupied Ce 4f have overlap in the bottom of conduction band, they are less effective in transferring electrons and photocatalytic activities for their high localized nature. The activities for H_2 evolution on $K_4Ce_2Ta_{10}O_{30}$ are more excellent than that on $K_4Ce_2Nb_{10}O_{30}$, although the band gap of $K_4Ce_2Nb_{10}O_{30}$ (1.8 eV) is narrower than that of $K_4Ce_2Ta_{10}O_{30}$ (2.3 eV). This is because while the both photocatalysts have the similar level in the top of valence band, the bottom of conduction band for $K_4Ce_2Nb_{10}O_{30}$ locates too close to the NHE potential (H^+/H_2 level), resulting in the driving force for water reduction is smaller correspondingly. These findings provide interesting information to develop new photocatalysts responsive to visible light.

Acknowledgements

This work was financially supported by the National Natural Science Foundation of China (Grant No. 50076026), the National Key Basic Research and Development Program (Grant No. 2003CB214500) and the Trans-Century Training Programme Foundation for the Talents from Chinese Ministry of Education.

References

[1] A. Fujishima, K. Honda, Nature 238 (1972) 37.
[2] T. Ishii, H. Kato, A. Kudo, J. Photochem. Photobiol. A: Chem. 163 (2004) 181.
[3] K. Sayama, A. Tanaka, K. Domen, K. Maruya, T. Onishi, J. Phys. Chem. B 95 (1991) 1345.
[4] H. Kato, A. Kudo, Catal. Taday 78 (2003) 561.
[5] Y. Miseki, H. Kato, A. Kudo, Chem. Lett. 34 (2005) 54.
[6] J. Sato, N. Saito, H. Nishiyama, Y. Inoue, J. Phys. Chem. B 15 (2001) 6051.
[7] J. Sato, H. Kobayashi, K. Karashi, N. Saito, H. Nishiyama, Y. Inoue, J. Phys. Chem. B 108 (2004) 4369.
[8] A. Kudo, K. Omori, H. Kato, J. Am. Chem. Soc. 121 (1999) 11459.
[9] W. Shangguan, A. Yoshida, J. Phys. Chem. B 106 (2002) 12227.
[10] A. Kudo, H. Kato, I. Tsuji, Chem. Lett. 33 (2004) 1534.
[11] K. Maeda, T. Takata, M. Hara, N. Saito, Y. Inoue, H. Kobayashi, K. Domen, J. Am. Chem. Soc. 127 (2005) 8262.
[12] H. Kato, A. Kudo, J. Phys. Chem. B 106 (2002) 5029.
[13] R. Asahi, T. Morikawa, T. Ohwaki, K. Aoki, Y. Taga, Science 293 (2001) 269.
[14] M. Hara, G. Hitoki, T. Takata, J.N. Kondo, H. Kobayashi, K. Domen, Catal. Today 78 (2003) 555.
[15] G. Hitoki, A. Ishikawa, T. Takata, J.N. Kondo, M. Hara, K. Domen, Chem. Lett. 6 (2002) 736.
[16] M. Liu, W. You, Z. Lei, G. Zhou, J. Yang, G. Wu, G. Ma, G. Luan, T. Takata, M. Hara, K. Domen, C. Li, Chem. Commun. (2004) 2192.
[17] T. Ohno, M. Akiyoshi, T. Umebayashi, K. Asai, T. Mitsui, M. Matsumura, Appl. Catal. A: Gen. 265 (2004) 115.
[18] T. Ohno, T. Tsubota, Y. Nakamura, K. Sayama, Appl. Catal. A: Gen. 288 (2005) 74.
[19] H.G. Kim, D. Hwang, J. Lee, J. Am. Chem. Soc. 126 (2004) 8912.
[20] M. Machida, J. Yabunaka, T. Kijima, S. Mastsushima, M. Arai, Int. J. Inorg. Mater. 3 (2001) 545.
[21] Z. Zou, H. Arakawa, J. Photochem. Photobiol. A: Chem. 158 (2003) 145.

[22] A. Kudo, H. Okutomi, H. Kato, Chem. Lett. (2000) 1212.
[23] F. Brik, R. Enjalbert, C. Roucau, J. Galy, J. Solid State Chem. 122 (1996) 7.
[24] Z. Zou, J. Ye, K. Sayama, H. Arakawa, Nature 414 (2001) 625.
[25] W. Shangguan, A. Yoshida, Int. J. Hydrogen Energy 24 (1999) 425.
[26] K. Ikarashi, J. Sato, H. Kobayashi, H. Saito, H. Nishiyama, Y. Inoue, J. Phys. Chem. B 106 (2002) 9048.
[27] H. Kato, A. Kudo, Chem. Phys. Lett. 295 (1998) 487.
[28] J.M. Sohn, S.I. Woo, Appl. Catal. A: Gen. 249 (2003) 375.
[29] H. Kato, A. Kudo, J. Phys. Chem. B 105 (2001) 4285.
[30] Z. Zou, J. Ye, H. Arakawa, K. Sayama, Nature 414 (2001) 625.
[31] A. Kudo, H. Kato, S. Nakagawa, J. Phys. Chem. B 104 (2000) 571.
[32] J. Ye, Z. Zou, H. Arakawa, M. Oshikiri, M. Shimoda, A. Matsushita, T. Shishido, J. Photochem. Photobiol. A: Chem. 148 (2002) 79.
[33] Z. Zou, Y. Ye, H. Arakawa, Int. J. Hydrogen Energy 28 (2003) 663.
[34] M.D. Segall, L.D. Lindan, M.J. Probert, C.J. Pickard, P.J. Hasnip, S.J. Clark, M.C. Payne, J. Phys.: Condens. Matter 14 (2002) 2717.
[35] J. Sato, N. Saito, Y. Yamada, K. Maeda, T. Takata, J.N. Kondo, M. Hara, H. Kobayashi, K. Domen, Y. Inoue, J. Am. Chem. Soc. 127 (2005) 4150.
[36] A. Ishikawa, T. Takata, T. Matsumura, J.N. Kondo, M. Hara, H. Kobayashi, K. Domen, J. Phys. Chem. B 108 (2004) 2637.
[37] A. Ishikawa, T. Takata, J.N. Kondo, M. Hara, H. Kobayashi, K. Domen, J. Am. Chem. Soc. 124 (2002) 13547.
[38] M. Machida, S. Murakami, T. Kijima, J. Phys. Chem. B 105 (2001) 3289.
[39] J. Ye, Z. Zou, H. Arakaw, M. Oshikiri, M. Shimoda, A. Matsushita, T. Shishido, J. Photochem. Photobiol. A: Chem. 148 (2002) 79.